SIGNAL TRANSDUCTION

Epac1 inhibition ameliorates pathological angiogenesis through coordinated activation of Notch and suppression of VEGF signaling

Hua Liu[1]*, Fang C. Mei[2,3]*, Wenli Yang[2,3]*, Hui Wang[2,3†], Eitan Wong[4], Jingjing Cai[1], Emma Toth[2,3], Pei Luo[2,3], Yue-Ming Li[4], Wenbo Zhang[1,5‡], Xiaodong Cheng[2,3‡]

In this study, we investigated the roles of Epac1 in pathological angiogenesis and its potential as a novel therapeutic target for the treatment of vasoproliferative diseases. Genetic deletion of Epac1 ameliorated pathological angiogenesis in mouse models of oxygen-induced retinopathy (OIR) and carotid artery ligation. Moreover, genetic deletion or pharmacological inhibition of Epac1 suppressed microvessel sprouting from ex vivo aortic ring explants. Mechanistic studies revealed that Epac1 acted as a previously unidentified inhibitor of the γ-secretase/Notch signaling pathway via interacting with γ-secretase and regulating its intracellular trafficking while enhancing vascular endothelial growth factor signaling to promote pathological angiogenesis. Pharmacological administration of an Epac-specific inhibitor suppressed OIR-induced neovascularization in wild-type mice, recapitulating the phenotype of genetic Epac1 knockout. Our results demonstrate that Epac1 signaling is critical for the progression of pathological angiogenesis but not for physiological angiogenesis and that the newly developed Epac-specific inhibitors are effective in combating proliferative retinopathy.

INTRODUCTION

The vascular system supports tissue growth and organ function in vertebrates. While vasculogenesis, the process of generating blood vessels de novo from angioblasts, is essential for embryonic development, angiogenesis, the formation of new blood vessels from existing vasculature, is a double-edged sword. On one hand, physiological angiogenesis is vital for normal growth and development, as well as for female reproductive processes and wound healing. On the other hand, pathological angiogenesis plays important roles in abnormal vessel growth, which contributes to the pathogenesis of diverse human diseases such as retinopathy of prematurity (ROP), diabetic retinopathy, cancer, and cardiovascular disorders (*1*). Understanding the molecular mechanisms of angiogenesis is critical for developing effective anti- or pro-angiogenic therapeutics.

Cyclic adenosine monophosphate (cAMP), a pleotropic second messenger, is an important stress response signal that had previously been shown to regulate many physiological and pathophysiological processes. Exchange proteins directly activated by cAMP (Epac) are major intracellular sensors for cAMP, independent of the classic cAMP receptor, protein kinase A (PKA) (*2*). In mammals, there are two Epac isoforms, Epac1 and Epac2, encoded by two separated genes, acting as guanine nucleotide exchange factors for the Ras-related small guanosine triphosphatases (GTPases) Rap1 and Rap2 (*3*, *4*). Epac1 is ubiquitously expressed and often involved in pathological conditions such as cardiac hypertrophy and obesity, while Epac2 is mainly involved in physiological processes such as insulin secretion, learning, and memory (*5*). Epac1 is highly abundant in blood vessels, particularly in endothelial cells (ECs) (*6*), where Epac1 signaling has been shown to regulate cell adhesion, migration, junction formation, and endothelial barrier functions (*7*–*10*). In addition, Epac1 activation induces Weibel-Palade body exocytosis (*11*) while suppressing annexin A2 cell surface translocation in ECs (*12*). Whereas Epac1 knockout (KO) mice have increased microvascular permeability (*13*), deletion of Epac1 in mice protects animals from fatal rickettsioses by blocking bacterial adhesion and invasion into the endothelial lining of the blood vessels (*14*). Despite extensive studies of Epac1 functions in ECs (*5*, *6*), the specific roles of Epac1 in angiogenesis have not been prudently explored and remain unclear. Limited recent investigations using *Epac1* KO mice have generated contradictory phenotypes (*15*, *16*). While Garg and colleagues concluded that deletion of Epac1 protected mice retina from oxygen-induced vascular damage (*15*), Epac1 was shown to protect the retina against ischemia-reperfusion–induced neuronal and vascular damage (*16*).

In this study, we describe a previously unknown endothelial function of Epac1, in which Epac1 acts as a previously unidentified inhibitor of the γ-secretase/Notch signaling pathway while enhancing vascular endothelial growth factor (VEGF) signaling to promote pathological but not physiological angiogenesis. Moreover, we demonstrate that pharmacological inhibition of Epac provides beneficial therapeutic effects by ameliorating pathological angiogenesis in mouse model of ROP.

RESULTS

Epac1 modulates pathological but not physiological angiogenesis in the retina

Epac1 is highly expressed in vascular tissues, particularly in vascular EC and vascular smooth muscle cell (vSMC). To determine whether Epac1 regulates angiogenesis, we assessed retinal vascular development of wild-type (WT) and *Epac1*$^{-/-}$ littermates at the early developmental

[1]Department of Ophthalmology and Visual Sciences, University of Texas Medical Branch, Galveston, TX, USA. [2]Department of Integrative Biology and Pharmacology, University of Texas Health Science Center, Houston, TX, USA. [3]Texas Therapeutics Institute, University of Texas Health Science Center, Houston, TX, USA. [4]Chemical Biology Program, Memorial Sloan Kettering Cancer Center, New York, NY, USA. [5]Department of Neuroscience, Cell Biology and Anatomy, University of Texas Medical Branch, Galveston, TX, USA.
*These authors contributed equally to this work.
†Present address: Department of Pathology, University of Texas Medical Branch, Galveston, TX, USA
‡Corresponding author. Email: we2zhang@utmb.edu (W.Z.); xiaodong.cheng@uth.tmc.edu (X.C.)

stage. Retinal superficial vessels start to radially sprout from the optic disc right after birth and extend toward the periphery, which is completed at postnatal day 8 (P8). We found that the retinas from WT and *Epac1*$^{-/-}$ mice displayed comparable vascularization at P5 (fig. S1), suggesting that Epac1 is dispensable for physiological angiogenesis.

To investigate whether Epac1 is important for angiogenesis under pathological conditions, we used a mouse model of oxygen-induced retinopathy (OIR) that has been widely used to study mechanisms of retinal pathological angiogenesis as seen in ROP and diabetic retinopathy (*17*, *18*). In this model, P7 pups along with their nursing mother were exposed to 70% oxygen (hyperoxia) for 5 days (P7 to P12) to induce vascular obliteration in the central retina. At P12, mice were returned to room air (relative hypoxia) to induce pathological neovascularization (Fig. 1A). Compared with normal vessels, neovascular tufts have stronger fluorescent intensity, and protrude into the vitreous with shapes as clump or small ball (Fig. 1B). In this model, the level of cAMP was significantly increased in relative hypoxia retinas compared with room air controls (Fig. 1C), which is consistent with the finding that the levels of phosphodiesterases (PDEs) 1b, 3a, and 3b were down-regulated in OIR retinal vasculature (fig. S2, B to D). Furthermore, while the expression level of PKA catalytic subunit was not affected (fig. S2E), the levels of Epac1 mRNA and protein were markedly increased in retinal vessels from OIR mice (Fig. 1, D and E). A similar increase in Epac2 expression was also observed (fig. S2F). These observations signify that cAMP/Epac signaling might be involved in modulating pathological angiogenesis.

Next, we examined vascular phenotypes of WT and *Epac1*$^{-/-}$ mice that underwent OIR treatment. At P12, a time point maximum vascular regression that occurs in OIR, WT and *Epac1*$^{-/-}$ retinas exhibited indistinguishable vascular obliteration (Fig. 1, F and G), indicating that *Epac1* deletion does not affect the vulnerability of retinal vasculature to oxygen. On the other hand, we found that *Epac1*$^{-/-}$ retinas exhibited a significant reduction in pathological neovascularization compared with WT retinas at P17, a time point when retinal neovascularization reaches its maximum extent (Fig. 1, H to J). Similar results were obtained by examining neovascularization (preretinal vessels) in retinal sections (Fig. 1K) (*19*). The reduced OIR neovascular response observed in *Epac1* KO mice was unlikely due to developmental changes, as the body weights of WT and *Epac1*$^{-/-}$ OIR mice were identical at P17 (fig. S1D). In contrast,

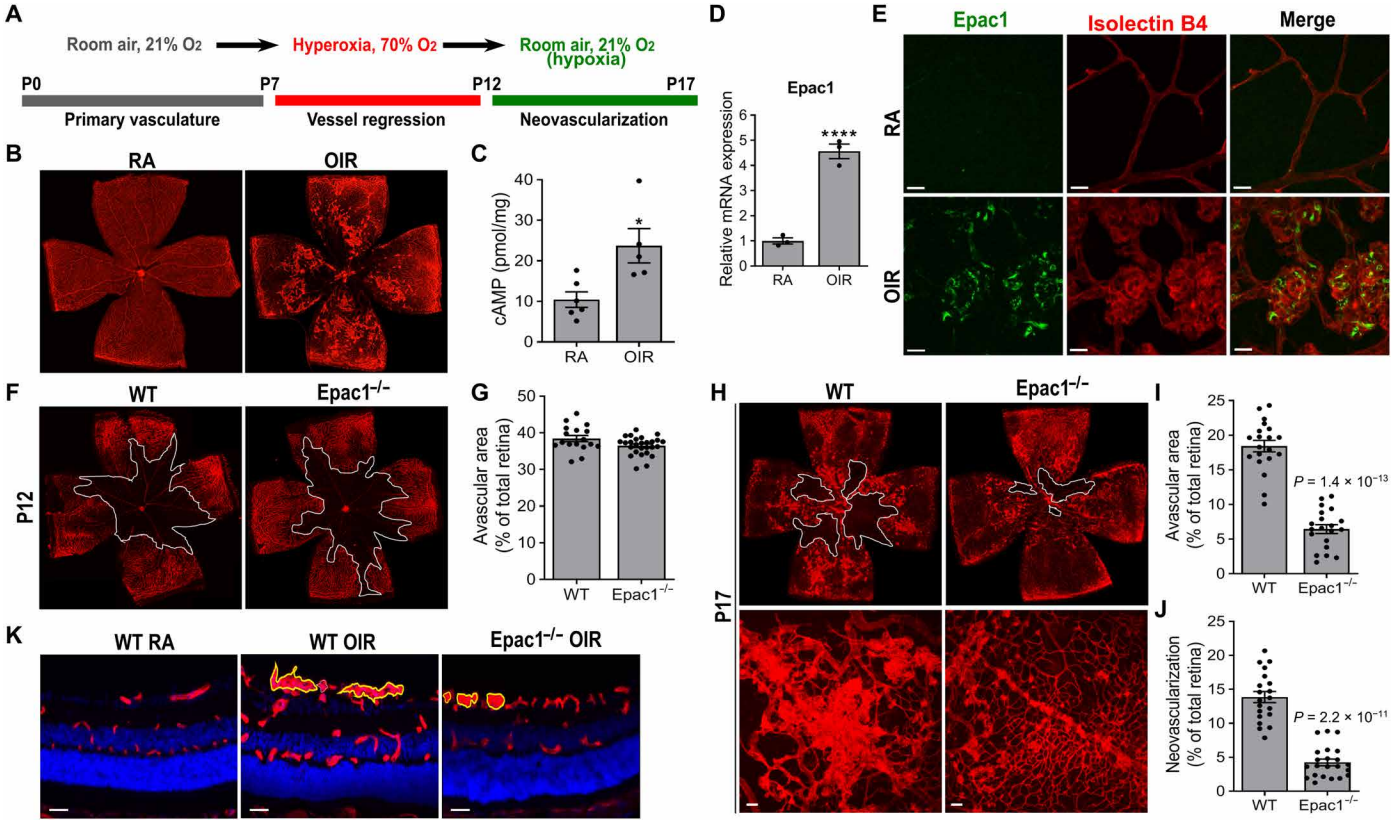

Fig. 1. Epac1 expression is enriched in retinal blood vessels of OIR mice, and *Epac1* deletion prevents OIR-induced neovascularization. (**A**) A schematic diagram depicting the mouse OIR model. Pups along with their nursing mother were exposed to 70% oxygen from P7 to P12 to induce vessel regression and returned to room air (RA) from P12 to induce pathologic neovascularization, which peaks at P17. (**B**) Representative images of retinal vasculature of WT mice from room air and OIR at P17. (**C**) Level of cAMP in retinas of WT mice from RA and OIR at P14. $n = 5$ to 6. *$P < 0.05$ compared with RA. (**D**) Expression of Epac1 mRNA in retinal vasculature isolated from WT RA and OIR mice at P17. $n = 3$; each n represents a pool of six retinas. ****$P < 0.001$ compared with RA. (**E**) Confocal images of immunostaining of Epac1 (green) in retinal vasculature of WT RA and OIR mice at P17. (**F**) Retinal vasculature from P12 WT and *Epac1*$^{-/-}$ OIR mice. White lines outline the area of vaso-obliteration. (**G**) Graph represents avascular area at P12. $n = 17$ to 27. (**H**) Representative retinal vasculature (top) and high magnification images (bottom) from P17 WT and *Epac1*$^{-/-}$ OIR mice. (**I** and **J**) Graphic representation of avascular and neovascularization area from WT and *Epac1*$^{-/-}$ OIR mice at P17. $n = 20$. (**K**) Retinal sections of WT and *Epac1*$^{-/-}$ OIR mice at P17. Yellow lines outline neovascularization. Red, isolectin B4 staining for vessel; blue, DAPI (4′,6-diamidino-2-phenylindole) staining for nuclei. Scale bars, 50 μm.

Epac2 deletion did not affect this process (fig. S3). *Epac1* deletion also reduced avascular area (Fig. 1I), indicating increased physiological vascular repair in these mice. Thus, these findings support the notion that Epac1, rather than Epac2, is critically implicated in cAMP-mediated pathological angiogenesis.

To assess whether these vascular differences in WT and *Epac1*$^{-/-}$ mice are brought about by differential proliferation of ECs, we performed immunostaining of whole-mount retinas with antibody against phospho–histone H3 (Ser^{10}), which is a marker for labeling proliferative cells. Following exposure to OIR, WT retina exhibited a large number of phospho–histone H3–positive cells, which was markedly decreased in the *Epac1*$^{-/-}$ retina at P15 and P17 (fig. S4). This finding indicates that *Epac1* deletion suppresses the proliferation of ECs during the process of neovascularization.

Epac1 promotes neovascularization during stenosis in response to vascular injury

Consistent with the aforementioned protective effect of *Epac1* deletion on pathological neovascularization in the retina, our recent study demonstrates that in response to vascular injury, *Epac1*$^{-/-}$ mice show a significantly reduced neointimal hyperplasia when compared with their WT littermate controls (*20*). In addition to reported neointimal formation, careful histological analysis revealed significant neovascularization in WT samples, manifested by the formation of microvessels, mostly in the outer layer of media/adventitia, in response to carotid artery ligation. On the other hand, minimal neovascularization was observed in *Epac1*$^{-/-}$ arteries, which retained their regular vascular structure with minimal neointimal formation (Fig. 2A). Neovascularization in WT samples was confirmed by immunofluorescence staining of EC- and vSMC-specific markers using BS1 lectin–fluorescein isothiocyanate (FITC) or anti–α–smooth muscle actin (α-SMA) antibody, respectively (Fig. 2B). On average, 14 to 19 microvessels could be detected in each WT ligated carotid artery section, while only 1 or 2 were presented in *Epac1*$^{-/-}$ counterparts (Fig. 2C). Together, these results suggest that Epac1 contributes to pathogenic angiogenesis in both microvascular and macrovascular systems during vascular remodeling.

Loss of *Epac1* in mice reduces vascularization in Matrigel plug assay

To further define the role of Epac1 in angiogenesis under pathological conditions mimicking ischemia and inflammation, we performed a Matrigel plug angiogenesis assay by injecting VEGF/fibroblast growth factor (FGF)–containing Matrigel subcutaneously into the ventral region of *Epac1*$^{-/-}$ and WT mice. The Matrigel plugs harvested from WT mice were dark and opaque, indicating a robust blood perfusion. On the other hand, the Matrigel plugs retrieved from *Epac1*$^{-/-}$ mice remained semitransparent and with mostly sparse and superficial blood perfusion (Fig. 2D). Hematoxylin and eosin (H&E) staining was further performed to examine the blood vessel formation within the plugs. Blood vessel–like structures and abundant blood cells were obvious in WT Matrigel plugs. However, vessel-like structures and blood cells were mostly absent in *Epac1*$^{-/-}$ Matrigel plugs (Fig. 2E). Costaining of EC and vSMC cell markers revealed that ECs in WT plugs formed a regular pattern, lining along the vessel as seen in normal vascular structure with most of the ECs surrounded by α-SMA–positive vSMCs, whereas ECs in *Epac1*$^{-/-}$ plugs were abundant but mostly disorganized and scattered, and there were markedly less supporting vSMCs (Fig. 2F). These data are in agreement with the reduced retinal neovascularization in response to vascular injury observed in *Epac1*$^{-/-}$ mice, indicating that deletion of *Epac1* inhibits inflammatory neovascularization in mice.

Epac1 deletion suppresses vascular sprouting ex vivo

To further dissect the cellular function of Epac1 in angiogenesis, we performed a classical ex vivo angiogenesis assay using mouse aortic rings isolated from *Epac1*$^{-/-}$ and WT mice. Unlike most in vitro assays that are only suitable for studying a particular step of the angiogenesis, the aortic ring assay recapitulates all the key steps of in vivo angiogenesis, allowing an in-depth dissection of the contribution of individual cellular processes such as proliferation, migration, tube formation, microvessel branching, perivascular recruitment, and remodeling (*21*). As shown in Fig. 2 (G to H), we observed robust capillary sprouting and branching of vessel outgrowth for aortic rings from WT mice. In contrast, aortic rings from *Epac1*$^{-/-}$ mice exhibited only minimum sprouting vessel outgrowth. The few sprouts grown from *Epac1*$^{-/-}$ aortic rings were significantly shorter, thinner, and had fewer branches. The failure of *Epac1*$^{-/-}$ aortic rings to form endothelial sprouts is in agreement with the in vivo results and suggests that Epac1 is important for pathological angiogenesis and that deletion of Epac1 suppresses neovascularization. A similar inhibitory effect on aortic microvessel sprouting was observed by pharmacological inhibition using an Epac-specific inhibitor ESI-09 (*22*, *23*), which dose-dependently suppressed microvessel outgrowths in WT aortic rings (fig. S5).

Epac1 promotes endothelial angiogenic potential through cross-talk with VEGF signaling

Endothelial proliferation, migration, and tube formation in response to VEGF stimulations are key processes during angiogenesis. We then explored whether alterations of Epac1 signaling in ECs affect their angiogenic abilities. Using MTS [3-(4,5-dimethylthiazol-2-yl)-5-(3-carboxymethoxyphenyl)-2-(4-sulfophenyl)-2H-tetrazolium] assay, scratch wound healing assay, and tube formation on Matrigel and three-dimensional (3D) angiogenesis assays, we found that in the presence of a membrane-permeable Epac-specific activator, 8-(4-chlorophenylthio)-2′-*O*-methyladenosine-3′,5′-cyclic monophosphate acetoxymethyl ester (007-AM or 8-pCPT-2-O-Me-cAMP-AM), ECs displayed increases in proliferation (fig. S6A), migration (fig. S6B), and tube formation (fig. S6, C and D) in a similar manner as in response to VEGF stimulation. In contrast, inhibition of Epac signaling by a selective Epac inhibitor, ESI-09, markedly decreased EC's ability to proliferate (fig. S6A), migrate (fig. S6B), and form a capillary-like structure on Matrigel (fig. S6, C and D) under both basal and VEGF- or 007-AM–stimulated conditions. In addition, activation of Epac by 007-AM promoted cell migration and invasion through the Matrigel in a transwell assay (fig. S6, E and G), while ESI-09 treatment suppressed the migration-invasion potential (fig. S6, F and H). Moreover, in a 3D angiogenesis assay that mimics the vessel formation, inhibition of Epac1 in human umbilical cord endothelial cells (HUVECs) by ESI-09 or by small interfering RNA (siRNA) resulted in a significant decrease in vessel structures (Fig. 3, A to D). Together, these data demonstrate that Epac activation in ECs is sufficient to enhance angiogenic properties, leading to pathological angiogenesis.

Considering the paramount importance of VEGF signaling in angiogenesis and EC functions, we investigated whether Epac1 might be involved in regulating VEGF-mediated signaling in ECs. As shown in Fig. 3E, activation of Epac by 007-AM promoted the activation of

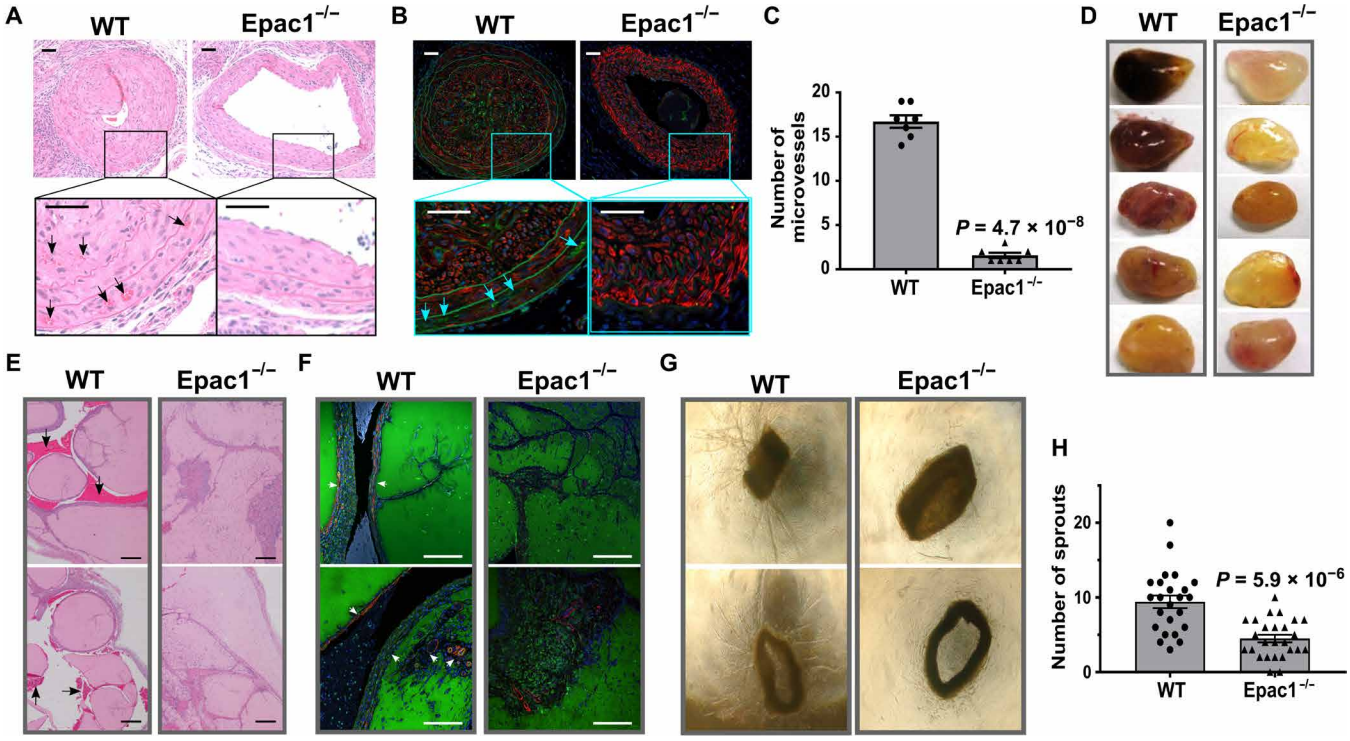

Fig. 2. Epac1 deficiency impairs pathological neovascularization. (**A**) Hematoxylin and eosin (H&E) staining of ligated carotid artery sections from WT and *Epac1*$^{-/-}$ mice. (**B**) Immunofluorescence-stained ligated carotid artery sections from WT and *Epac1*$^{-/-}$ mice. Green, BS1 lectin-FITC; red, α-SMA; blue, DAPI. Arrows indicate neovascularization. Scale bars, 50 μm. (**C**) Quantification of neovascularization in ligated carotid artery sections from WT and *Epac1*$^{-/-}$ mice ($n = 7$). (**D**) Images of subcutaneously implanted Matrigel plugs retrieved from WT and *Epac1*$^{-/-}$ mice. (**E**) H&E staining of sectioned Matrigel plugs harvested from WT and *Epac1*$^{-/-}$ mice. Note the presence of microvessel-like structures and abundant blood cells (arrows) in WT Matrigel plugs, which were mostly absent in *Epac1*$^{-/-}$ Matrigel plugs. Scale bars, 200 μm. (**F**) Confocal images of immunofluorescence-stained, sectioned Matrigel plug slides harvested from WT and EPAC1$^{-/-}$ mice. Green, BS1 lectin-FITC; red, α-SMA; blue, DAPI. Arrows, microvessel-like structures. Scale bars, 200 μm. (**G**) Representative images of microvessel outgrowths in VEGF/FGF-treated aortic rings isolated from WT and *Epac1*$^{-/-}$ mice. (**H**) Quantification of main microvessel sprouts observed from WT ($n = 24$) and *Epac1*$^{-/-}$ ($n = 26$) aortic rings.

Akt and endothelial nitric oxide synthase (eNOS), two prominent VEGF signaling downstream readouts, when administrated alone and further synergized VEGF-mediated activation of Akt and eNOS when administrated in combination. On the other hand, knocking down Epac1 in ECs suppressed basal and VEGF-stimulated phospho-Akt and phospho-eNOS (Fig. 3F). Together, these data suggest that Epac1 activation promotes and synergizes with VEGF signaling. These findings are consistent with Epac1's in vivo functions in promoting pathological angiogenesis.

To determine whether Epac1-mediated Akt and eNOS phosphorylation is Rap1 dependent, we tested the effect of Rap1GAP, a Rap1-specific GTPase-activating protein that efficiently keeps Rap1 in its inactive guanosine diphosphate–bound state. Ectopic expression of Rap1GAP in HUVECs suppressed cellular Rap1–uanosine triphosphate level (fig. S6I). Rap1GAP blocked the ability of 007-AM to stimulate Akt and eNOS phosphorylation (fig. S6J), consistent with our previous finding in 3T3-L1 cells (*24*). These results suggest that Rap1 is required for Epac-induced Akt and eNOS activation in HUVECs.

Epac1 controls Notch signaling

Given that Notch signaling plays a critical role in regulating angiogenesis, particularly by balancing the proangiogenic effect of VEGF signaling (*25*), we examined the status of Notch signaling in ECs in response to Epac1 inhibition or activation. As shown in Fig. 4A, gene silencing of Epac1 increased the levels of mRNAs for Notch target genes Hes1 and Hey1, as well as Notch ligand DLL4, whose expression is also induced by Notch activation (*26*). Conversely, activation of Epac1 in ECs by 007-AM down-regulated the expression of these genes (Fig. 4B). These results suggest that Epac1 negatively regulates Notch signaling in ECs. Consistent with this notion, knocking down Epac1 in ECs led to a significant decrease in the cellular protein level of Notch1 and concomitant increases in the intracellular domain of Notch protein (NICD) and its target gene DLL4 at the protein level (Fig. 4C). In HUVECs, two protein bands with apparent molecular weight around 300 and 120 kDa, corresponding to the full-length protein (Notch1-FL) and the cleaved transmembrane/intracellular region (Notch1-NTM), were revealed by the anti-Notch1 antibody. Since the 300-kDa band was much weaker than the 120-kDa one and the expression pattern for Notch1-FL and Notch1-NTM followed the same trend, we used the Notch1-NTM band for protein quantification. To address whether the effects of Epac1 on Notch signaling are related to its guanine nucleotide exchange activity, i.e., Rap1, we suppressed cellular Rap1 activity by ectopic expression of Rap1GAP and found that it down-regulated cellular Notch1, NICD, and Notch target gene expression (Fig. 4, D and E), which is opposite to those observed by silencing *Epac1*. These results suggest that the effects of *Epac1* on Notch signaling are not dependent on Rap1 regulation.

To confirm that the apparent Notch activation observed in ECs with *Epac1* silencing was also occurring in vivo, we isolated mRNA from retinal vasculature harvested from WT and *Epac1*$^{-/-}$ OIR mice

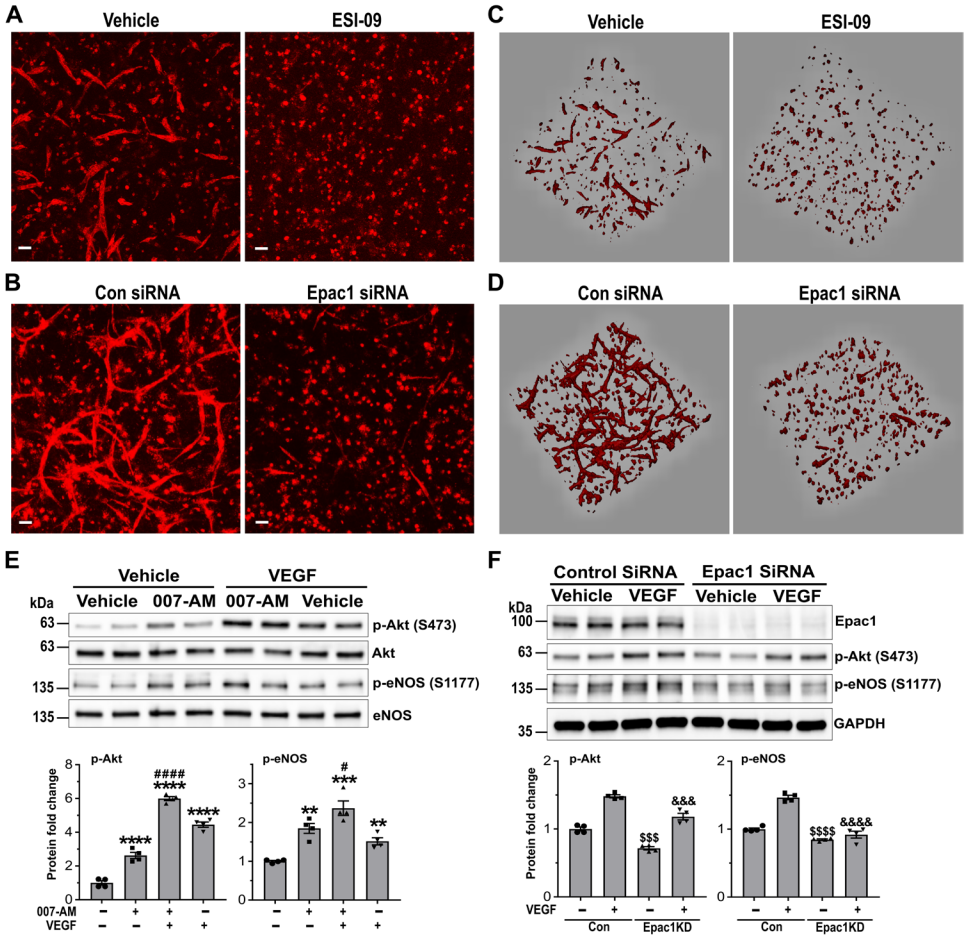

Fig. 3. Epac1 cross-talks with VEGF signaling and regulates EC functions. (**A** and **B**) Images of 3D angiogenesis assay of HUVECs, which were cultured alone but treated with vehicle or 2.5 μM ESI-09 (A), or transfected with control siRNA or Epac1 siRNA and then cocultured with fibroblasts (B) for 5 days. Red, isolectin B4 staining to highlight ECs. Scale bars, 50 μm. (**C** and **D**) 3D images of the same experiments shown in (A) and (B). (**E**) Activation of Epac1 by 007-AM (5 μM, 30 min) alone promoted phospho-Akt (S473) and phospho-eNOS (S1177) and synergized with VEGF (10 ng/ml, 30 min) in activating Akt and eNOS. Values are expressed as relative fold change in the format of means ± SEM ($n = 4$ independent experiments). $^{**}P < 0.01$, $^{***}P < 0.005$, $^{****}P < 0.001$; 007-AM–, VEGF-, or VEGF/007-AM–treated versus vehicle control; $\#P < 0.05$, $\#\#\#\#P < 0.001$; VEGF/007-AM–treated versus VEGF alone. (**F**) Gene silencing of Epac1 by siRNA (Epac1KD) decreased basal and VEGF (10 ng/ml, 30 min)–stimulated phospho-Akt (S473) and phospho-eNOS (S1177) activation. Values are expressed as relative fold change in the format of means ± SEM ($n = 4$ independent experiments). $\$\$P < 0.005$, $\$\$\$\$P < 0.001$; Epac1 siRNA versus control siRNA; $\&\&\&P < 0.005$, $\&\&\&\&P < 0.001$; VEGF-treated Epac1 siRNA versus VEGF-treated control siRNA. GAPDH, glyceraldehyde-3-phosphate dehydrogenase.

at P17 and monitored the expression of Notch target genes Hes1, Hye1, and DLL4. As shown in fig. S7A, the levels of Notch target genes were elevated in *Epac1*$^{-/-}$ OIR retinal vasculature. Similarly, we examined the expression levels of DLL4 in cells on Matrigel plug sections harvested from WT or *Epac1* KO mice using immunofluorescence staining. While specific DLL4 staining was observed in ECs costained by BS1 lectin-FITC in both WT and *Epac1* KO Matrigel plug sections (fig. S7B), the intensities of DLL4 staining in *Epac1* KO ECs were significantly stronger than those in WT ECs (fig. S7C), suggesting an enhanced DLL4 expression and Notch signaling in *Epac1* KO ECs. Together, these data demonstrated that *Epac1* negatively regulates Notch signaling during pathological angiogenesis in vivo.

Epac1 interacts with presenilin 1 and suppresses γ-secretase activity

The ability of Epac1 to regulate Notch1 and NICD levels reciprocally suggests that Epac1 may modulate Notch signaling via acting on γ-secretase, which proteolytically cleaves Notch receptors to release NICD (*27*). To test this hypothesis, we performed affinity pulldown of Epac1 using anti-FLAG M2 resin in HeLa cells ectopically expressing FLAG-tagged Epac1 protein. HeLa cells were used because they express little endogenous Epac1 protein, allowing us to study the interaction of exogenously expressed FLAG-tagged Epac1 with other intracellular partners at high efficiency. As shown in Fig. 5A, immunoprecipitation of Epac1-FLAG protein pulled down the catalytic subunit of γ-secretase, presenilin 1 (PS1), while these proteins were absent from control pulldown in HeLa cells transfected with an empty vector. To confirm the affinity pull-down results and to prove that Epac1 also interacts with PS1 in ECs, we performed affinity pulldown of HUVEC or HeLa cell lysate using purified recombinant glutathione *S*-transferase (GST)–tagged Epac1 (GST-Epac1) protein as a bait. PS1 was present in the GST-Epac1 pull-down fraction eluted by glutathione but not in the control GST pull-down fraction from HUVEC or HeLa cell lysate (Fig. 5B).

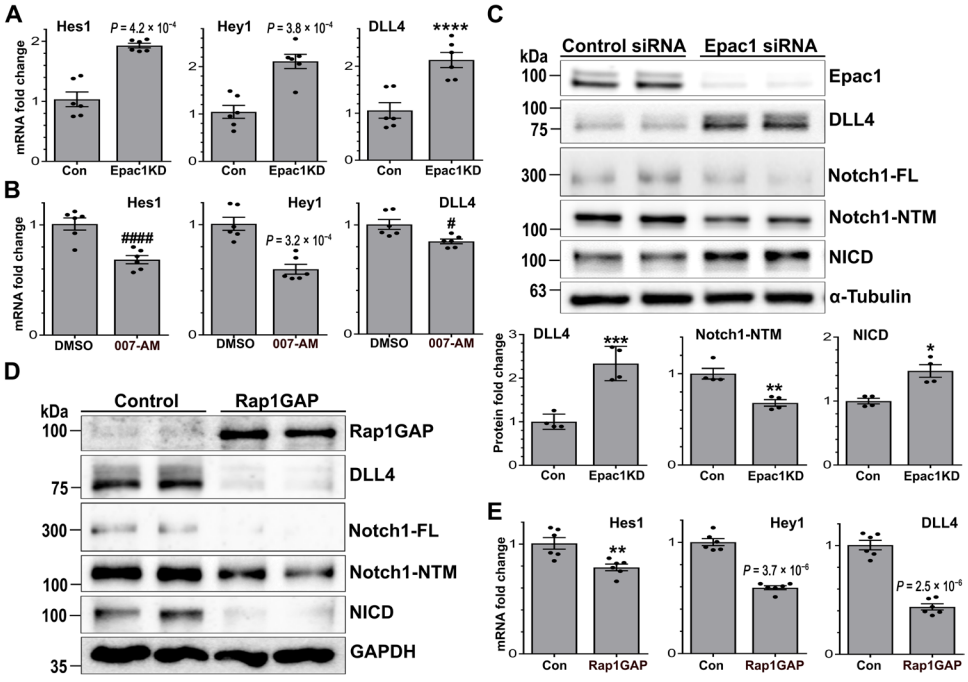

Fig. 4. Epac1 regulates Notch signaling in HUVECs. (**A**) Gene silencing of Epac1 by siRNA increased the mRNA expression of Notch target genes Hes1, Hey1, and DLL4. ****$P < 0.001$; Epac1 siRNA versus control siRNA. (**B**) Pharmacological activation of Epac1 by 007-AM (5 μM, 4 hours) suppressed the mRNA expression of Notch target genes Hes1, Hey1, and DLL4. #$P < 0.05$, ####$P < 0.001$; 007-AM versus dimethyl sulfoxide (DMSO) vehicle. (**C**) Gene silencing of Epac1 by siRNA decreased cellular protein level of Notch1 (Notch-FL and Notch1-NTM) while increasing the protein levels of NICD and DLL4. Values are expressed as relative fold change in the format of means ± SEM ($n = 3$ to 6 independent experiments). *$P < 0.05$, **$P < 0.01$, ***$P < 0.005$; Epac1 siRNA versus control siRNA. (**D**) Ectopic expression of Rap1GAP decreased cellular levels of DLL4, Notch1, and NICD. (E) Ectopic expression of Rap1GAP suppressed the mRNA expression of Notch target genes Hes1, Hey1, and DLL4. **$P < 0.01$.

To assess the functional importance of the interaction between Epac1 and PS1, we directly measured γ-secretase activity in response to Epac activation using an "exo-cell" γ-secretase assay that allows the monitoring of real-time cellular γ-secretase activity (*28*). Activation of Epac by stimulation of ECs with 007-AM (5 μM) led to a rapid and time-dependent reduction of γ-secretase activity (Fig. 5C). Pretreatment of ECs with 5 μM of ESI-09, an Epac-specific inhibitor, reversed 007-AM–induced reduction of γ-secretase activity (Fig. 5D), confirming that the suppressive effect of 007-AM on γ-secretase is indeed mediated by Epac. To further validate the results obtained in ECs, we performed similar experiments using HeLa cells that ectopically expressed human Epac1 (HeLa-Epac1). As shown in Fig. 5E, activation of *Epac1* by 007-AM in HeLa-Epac1 cells led to a comparable time-dependent reduction of γ-secretase activity, as observed in ECs. Again, ESI-09 pretreatment mitigated the inhibitory effect of 007-AM in HeLa-Epac1 cells (Fig. 5F). On the other hand, γ-secretase activity in parental HeLa cells, which express little Epac1, did not respond to treatment by either 007-AM or ESI-09 within the same time frame (fig. S8). Together, these results suggest that Epac1 interacts with γ-secretase and inhibits its cellular activity.

Epac1 regulates γ-secretase intracellular trafficking

Previous studies report that γ-secretase exerts its cleavage function at early endosome (*29*–*31*). To test whether Epac1 modulates cellular γ-secretase activity by regulating cellular trafficking of γ-secretase, we monitored the rate of γ-secretase internalization by reversible cell surface protein biotinylation. As shown in Fig. 5G, while treatment of HUVECs with 007-AM for 12 min had no effects on the total cellular level of PS1, administration of 007-AM significantly reduced the amount of internalized PS1 compared with vehicle control. These results suggest that Epac activation inhibits γ-secretase internalization. To further confirm that *Epac1* interacts with and regulates γ-secretase, we tracked the cellular localization of PS1 by performing immunofluorescence staining of ECs using a PS1-specific antibody that has been previously validated for immunofluorescence staining (*32*, *33*). In basal ECs treated with vehicle control, PS1 displayed a diffused punctate staining throughout the cytosol and nucleus. Treatment of ECs by 007-AM led to a marked redistribution of PS1 staining highlighted by plasma membrane accumulation of PS1 (Fig. 5H). These results suggest that Epac activation promotes cell surface accumulation of PS1, which is consistent with the cell surface protein biotinylation data. Together, these observations indicate that Epac1 interacts with γ-secretase and that activation of Epac1 suppresses γ-secretase activity by blocking its internalization.

Inhibition of γ-secretase by DAPT counters the effects of silencing Epac1

The ability of Epac1 to interact and suppress cellular γ-secretase activity prompted us to investigate whether inhibition of γ-secretase would be able to reverse the apparent Notch activation induced by Epac1 silencing. When Epac1 knockdown ECs were treated with N-[N-(3,5-Difluorophenacetyl)-L-alanyl]-S-phenylglycine t-butyl ester (DAPT), a γ-secretase–specific inhibitor (*34*), we observed that DAPT treatment abolished Epac1 silencing–induced DLL4 and NICD up-regulation while concomitantly increasing the level of Notch1-NTM (fig. S9A). Consistent with the changes in protein expression, treatment of Epac1 knockdown ECs with DAPT also blocked Epac1

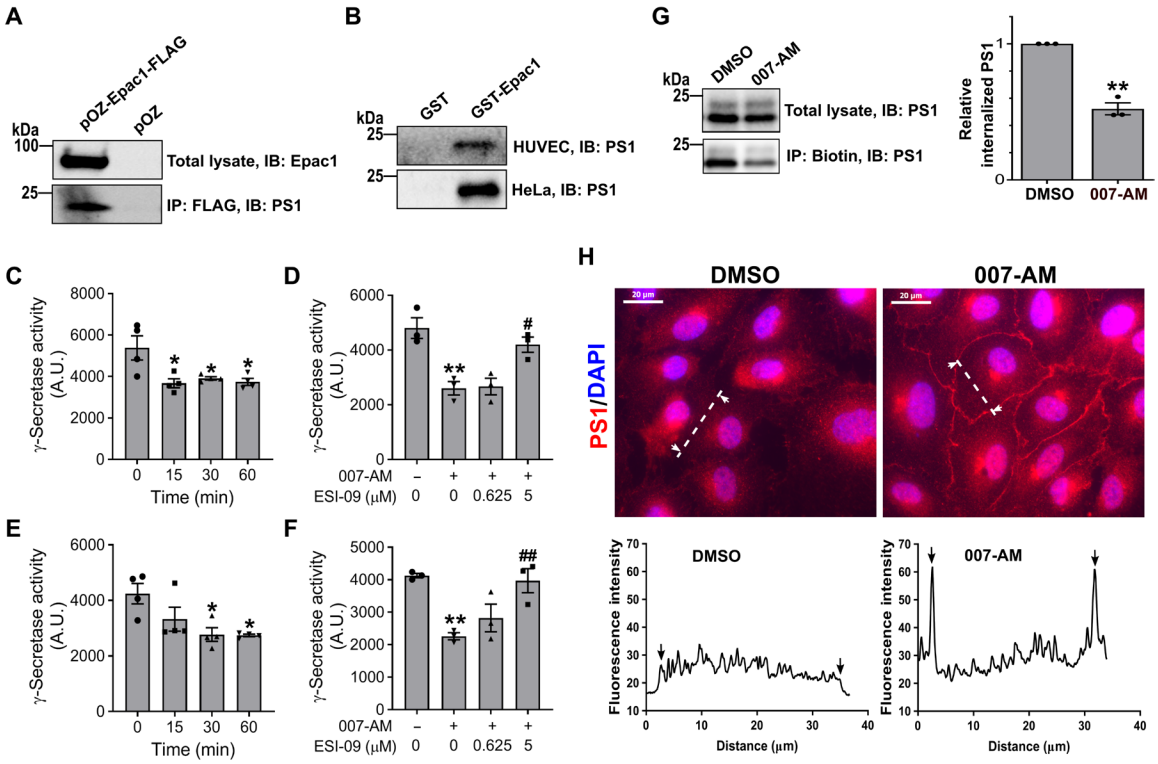

Fig. 5. Epac1 interacts with γ-secretase and inhibits its cellular activity. (**A**) Coimmunoprecipitation of Epac1 and γ-secretase. Affinity pulldown of Epac1 using anti-FLAG M2 resin in HeLa cells ectopically expressing *Epac1*-FLAG protein or control empty pOZ vector. Total cell lysates were probed by anti-Epac1 antibody, while immunoprecipitation (IP) was probed by an antibody specific for the catalytic subunit of γ-secretase, PS1. IB, immunoblotting. (**B**) Affinity pulldown of HUVEC or HeLa cell lysate by GST-Epac1 or GST control probed by an antibody specific for PS1. (**C** and **E**) *Epac1* activation reduces γ-secretase activity for Notch cleavage. γ-Secretase activity was assayed using recombinant Notch substrate in HUVECs (C) and HeLa-Epac1 cells (E). The enzymatic activity was measured following the treatment of 007-AM (5 μM) at different time points. Data are represented as AlphaLISA signal in arbitrary units (A.U.) in the format of means ± SEM ($n = 4$). Statistical analysis was done with one-way analysis of variance (ANOVA) compared to time point 0. *$P < 0.05$. (**D** and **F**) Epac1 inhibitor prevents the reduction of γ-secretase activity induced by 007-AM. HUVECs (D) and HeLa-Epac1 cells (F) were pretreated with ESI-09 at indicated concentrations. γ-Secretase activity was measured after incubation of 007-AM for 30 min. Values were represented as AlphaLISA in arbitrary units in the format of means ± SEM ($n = 3$). **$P < 0.01$ compared to vehicle control, ##$P < 0.01$ compared to 007-AM alone. (**G**) Levels of total cellular and internalized PS1 in HUVECs treated with 007-AM (5 μM) or DMSO for 12 min. Values were represented in the format of means ± SEM ($n = 3$). **$P < 0.01$ compared to vehicle control. (**H**) Immunofluorescence staining of cellular PS1 in HUVECs treated with 007-AM (5 μM) or DMSO for 12 min. Lower panels show the quantification of fluorescence intensity across the lines in the images. Arrows mark the locations of cell membrane. Scale bars. 20 μm.

silencing–induced Notch activation as demonstrated by the reduced mRNA expression of Notch target genes Hes1, Hey1, and DLL4 (fig. S9B). These results suggest that γ-secretase acts downstream of Epac1 to mediate its effect on Notch signaling.

To further test whether Epac1-mediated γ-secretase inhibition is responsible for the observed antiangiogenic effect in *Epac1* KO animals, we tested the ability of γ-secretase inhibition by DAPT to rescue the angiogenic defect associated with *Epac1* KO using the aforementioned ex vivo angiogenesis assay (*21*). As shown in fig. S10, aortic rings isolated from *Epac1* KO mice exhibited minimum sprouting vessel outgrowth as expected, while $Epac1^{-/-}$ aortic rings treated with DAPT showed a strong capillary sprouting and branching of vessel outgrowth. These results support the notion that *Epac1* inhibition, acting through γ-secretase, activates Notch signaling to suppress angiogenesis.

Pharmacological inhibition of Epac alleviates pathological angiogenesis in vivo

The ability of Epac1 to promote angiogenesis under pathological conditions provides opportunities for potential therapeutic intervention. To investigate the prospective of treating pathological angiogenesis by targeting Epac1, we subjected WT pups to OIR and treated them with vehicle or the Epac-specific inhibitor ESI-09 [20 mg kg^{-1} day^{-1} intraperitoneally] (*22*, *23*) from P12 to P16. Similar to *Epac1*-deficient mice, ESI-09 treatment significantly decreased the area of pathological neovascularization and enhanced vascular repair at P17 (Fig. 6, A to C), suggesting that Epac1 is a promising therapeutic target for the treatment of pathological angiogenesis.

DISCUSSION

Dysregulation of angiogenesis contributes to various pathogenic developments such as ocular and rheumatoid disorders, cardiovascular diseases, and cancer (*1*). While Epac1 is not essential for vasculature formation during embryonic development, as *Epac1* KO mice are viable and mature normally (*13*, *15*, *35*) and $Epac1^{-/-}$ mice have normal retinal developmental angiogenesis (fig. S1), our studies show that Epac1 signaling plays a crucial role in promoting angiogenesis under pathological conditions. Specifically, using a murine model of OIR for studying abnormal angiogenesis in the retina, we show that the expression of Epac1 is elevated in the vessel of ischemic retinas and that the deletion of *Epac1*, but not *Epac2*, prevents

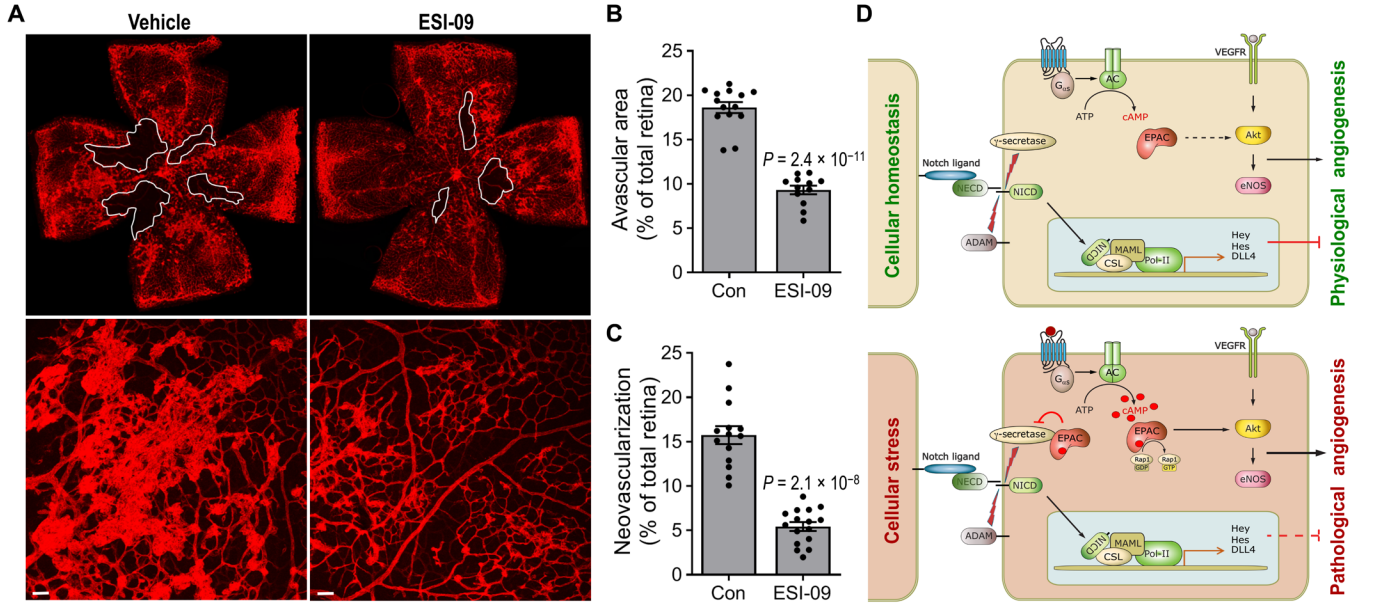

Fig. 6. Epac1 in pathological angiogenesis and as a therapeutic target for retinopathy. (**A**) Pharmacological inhibition of Epac prevents OIR-induced neovascularization. Representative retinal vasculature (top) and high-magnification images (bottom) at P17 in OIR mice treated with Epac inhibitor ESI-09 or vehicle (Con). White lines outline the area of vaso-obliteration. (**B** and **C**) Graphs represent avascular and neovascularization area at P17 ($n = 12$ to 16). (**D**) Epac1 promotes pathological angiogenesis through sensitization of VEGF signaling and suppression of Notch activation via γ-secretase inhibition. VEGFR, VEGF receptor.

OIR-induced neovascularization. The effect of *Epac1* deletion on reduced pathological angiogenesis is further supported by the observations of impaired angiogenic response to VEGF/FGF2 in Matrigel plugs implanted in *Epac1* null mice, decreased neovascularization during stenosis, and decreased microvessel sprouting from *Epac1* KO aortic rings.

These results have major clinical/therapeutic significances, as OIR is a proven model for human ophthalmic neovascular diseases including ROP, a leading cause of vision impairment and blindness in children. Current treatments for ROP, including laser photocoagulation, the standard of care for treating retinal neovascularization in ROP, and supplement cryotherapy used occasionally in severe cases (*36*), are invasive and destroy retinal neurons and impair peripheral vision. Anti-VEGF agents are used to treat neovascularization in age-related macular degeneration and have been used for treating ROP off label. However, they are not approved by the U.S. Food and Drug Administration for ROP therapy because of its potential interference with vasculogenesis and retinogenesis in premature infants. Our study suggests that Epac1 may represent a promising therapeutic target for ROP since *Epac1* deletion attenuates pathological angiogenesis but not physiological angiogenesis. This possibility is further supported by our data showing that pharmacological inhibition of Epac1 specifically suppresses OIR-induced neovascularization in WT mice and recapitulates the phenotype of genetic *Epac1* KO. Notably, blockade of Epac1 specifically inhibited pathological angiogenesis and changed the balance between pathological angiogenesis and physiological angiogenesis, resulting in less retinal neovascularization and more vascular repair (less avascular area). This feature is highly desirable in clinic, as current anti-VEGF agents block both pathological and physiological angiogenesis, and repeated injections are needed since retinal ischemia persists. This study warrants further investigation of the Epac1 pathway in ROP and other models of pathological angiogenesis and evaluation of the effects of newly developed Epac inhibitors.

Our study is in line with previous studies that blocking adenosine A2A receptor or β2-adrenergic receptor, which is coupled to $G_{\alpha s}$ protein to stimulate cAMP production, or activating somatostatin receptor 2, which is coupled to $G_{\alpha i}$ protein to inhibit cAMP production, prevents pathological retinal angiogenesis (*37*–*40*). In addition, it has been well documented that prostaglandin E2 promotes pathological angiogenesis (*41*) via $G_{\alpha s}$-coupled receptors EP2 and EP4 (*42*). Results from this study suggest that Epac1 may represent a common downstream effector responsible for mediating the cellular responses of the G_{α}/cAMP system on pathological angiogenesis.

Mechanistically, we found that Epac1 contributes to pathological neovascularization by modulating Notch and VEGF signaling, two key pathways for angiogenesis regulation (Fig. 6D). Neovascularization is initiated by the activation of EC, in response to an angiogenic trigger such as hypoxia, inflammation, or mechanical stress. Activation of EC leads to cell migration, proliferation and the formation of the initial capillary sprouts, on which the subsequent recruitment of vascular mural cells supports vessel stabilization and maturation (*43*). VEGF is a key positive regulator of endothelial proliferation and sprouting (*44*, *45*). On the other hand, the Notch signaling pathway counteracts the angiogenic sprouting effect of VEGF signaling (*25*, *46*). Stimulation of quiescent ECs by VEGF spearheads the vascular sprouting by promoting the formation of a tip cell, which guides the growth of new vascular sprout by integrating attractive and repulsive environmental cues (*47*). To prevent other ECs from turning into tip cells, a negative feedback regulation is imposed by Notch-mediated lateral inhibition, which down-regulates VEGF signaling in adjacent stalk cells to ensure the proper formation of a new vascular sprout connected to the existing vasculature (*48*). Our studies demonstrate that while Epac1 signaling is dispensable for angiogenesis under physiological conditions, dysregulation of the cAMP/Epac1 signaling under stress conditions promotes pathological angiogenesis through reciprocal cross-talks with the VEGF and Notch

signaling pathways by augmenting VEGF signaling while dampening Notch activation (Fig. 6D).

Activation of the phosphatidylinositol 3-kinase (PI3K)/Akt/eNOS pathway by cAMP/Epac1 signaling has been previously reported and is dependent on Rap1 (*49*, *50*). Our current study of Epac1's effects on vascular angiogenesis further confirms that Epac1 acts through Rap1 in cross-talking with the VEGF/PI3K/Akt/eNOS pathway. On the other hand, connection between Epac1 and Notch signaling has not been previously explored. Regulation of Notch signaling by Epac1 is not dependent on Rap1, as silencing Epac1 or Rap1 resulted in opposing effects on Notch receptor activation and target gene expressions. Instead, our study reveals a previously unknown Epac1 endothelial function, in which Epac1 regulates Notch signaling by modulating γ-secretase that is required for the activation of Notch signaling by proteolytic processing–activated Notch receptors to liberate NICD and allow transcriptional activation of Notch target genes (*27*). While PS proteins, nicastrin, anterior pharynx-defective 1, and PS enhancer 2 are the core components of the γ-secretase complex essential for basic enzymatic activity, cellular γ-secretase activity and specificity are modulated by additional regulatory proteins, such as TMP21, CD147, and HIF1α (*51*–*53*). Our findings that Epac1 modulates cellular γ-secretase activity by interacting directly with PS proteins and inhibiting their internalization identify Epac1 as a previously unidentified regulatory protein for γ-secretase.

In summary, our data provide compelling evidence that Epac1 is an important regulator of pathological angiogenesis. By modulating the cellular activity of γ-secretase, Epac1 suppresses the Notch signaling pathway and promotes angiogenesis under pathophysiological conditions. These results, coupled with the finding that pharmacological inhibition of Epac prevents OIR-induced neovascularization, suggest that Epac-specific inhibitors can be developed as promising therapeutics for the treatment of diseases associated with abnormal angiogenesis such as retinal vascular disorders, cancer metastasis, and other proliferative vascular diseases. Considering that Epac1 is a ubiquitous protein expressed in both vascular endothelial and smooth muscle cells, as well as in neurons, future studies using tissue-specific *Epac1* KO models are necessary to reveal the cell type–specific functions of Epac1. In addition, besides Epac1's roles in angiogenesis, recent studies also highlighted Epac1/Rap1's functions in retinal vascular permeability and laser-induced choroidal neovascularization (*54*, *55*). Dissecting the relative contributions of various Epac1's EC functions in the development of proliferative vascular disorders will help guide the development of more effective therapeutic strategies.

METHODS

Experimental animals

C57BL/6 mice were originally obtained from the Jackson Laboratory (Bar Harbor, ME). *Epac1*$^{-/-}$ and *Epac2*$^{-/-}$ mice on C57BL/6 background were generated as described previously (*35*, *56*). Animals were housed on a 12-hour light/12-hour dark cycle in pathogen-free facilities with ad libitum access to food and water. Both male and female littermates were used for this study. The use of all animals was in accordance with the National Institutes of Health guidelines and approved by the Institutional Animal Care and Use Committee of the University of Texas Health Science Center at Houston and University of Texas Medical Branch in Galveston. Pharmaceutical grade isoflurane (5%, inhalant) was used for animal euthanasia.

Oxygen-induced retinopathy

OIR was induced as previously described (*18*, *57*). Briefly, pups with their nursing mother were exposed to 70% oxygen from P7 to P12. Subsequently, they were returned to room air for 5 days to initiate rapid vessel growth and pathological neovascularization.

Immunostaining of whole-mount retinas

After mice were anesthetized at indicated time points, eyes were enucleated, fixed in 4% paraformaldehyde (PFA) overnight at 4°C, and dissected to isolate the retinas. Subsequently, the retinas were stained with antibodies against Epac1 (1:200; sc-8880, Santa Cruz Biotechnology, Santa Cruz, CA), phospho–histone H3 (1:200; 06-570, EMD Millipore, Billerica, MA), and/or Alexa Fluor 594–labeled isolectinB4 (*Griffonia simplicifolia*) (1:200; I21413, Thermo Fisher Scientific, Waltham, MA) to visualize vessels. After retinas were flat-mounted, images were captured by Zeiss LSM confocal microscopy or fluorescence microscopy. Avascular area and neovascularization were quantified as percentage of whole retinal area using ImageJ software.

Isolation of retinal vessels

Retinal vessels were isolated with a hypotonic shock method as previously described (*18*). Briefly, retinas were incubated in 5 to 6 ml of deionized water at 4°C for 1 hour followed by incubation in 4 ml of distilled water containing 500 U of deoxyribonuclease I (Worthington Biochemical, Lakewood, NJ) for 10 min. The nonvascular tissue was gently removed by repeatedly pipetting solution onto the retinal tissue.

Mouse carotid artery ligation injury model

Carotid artery ligation was performed on 10-week-old C57BL/6 WT and *Epac1*$^{-/-}$ littermates following a well-established protocol (*20*). Four weeks after the procedure, all animals were anesthetized and perfused with phosphate-buffered saline (PBS) and 10% formalin. The ligation-injured segments and contralateral noninjured carotid arteries were collected and fixed with 10% formalin, dehydrated, and embedded in paraffin. Neointimal lesion development was evaluated by H&E and immunofluorescence staining with α-smooth muscle actin-Cy3 antibody (C6198, Sigma-Aldrich, St. Louis, MO) and FITC-conjugated lectin from *Bandeiraea simplicifolia* (L9381, Sigma-Aldrich) as described previously (*20*).

In vivo Matrigel plug assay

Ice-cold Matrigel (400 μl; BD Biosciences, San Jose, CA) containing recombinant human VEGF (600 ng/ml; PeproTech, Rocky Hill, NJ) and FGF2 (300 ng/ml; PeproTech) was subcutaneously injected into the mouse groin area. Ten days after injection, Matrigel plugs were harvested, photographed, and then embedded in paraffin after being fixed in 10% formalin. Serial cross sections (5 μm) were cut for H&E and immunostaining analyses. To visualize blood vessel–like structures, Matrigel sections were stained for ECs and pericytes using an immunofluorescence protocol. Sections were first unmasked with citric antigen retrieval solution (Sigma-Aldrich) in a steamer for 20 min, blocked with 5% normal goat serum and 1% bovine serum albumin in PBS for 30 min, and stained with *B. simplicifolia* lectin conjugated with FITC for ECs (L9381, Sigma-Aldrich) and anti–α-SMA (C6198, Sigma-Aldrich) for pericytes or anti-DLL4 antibody (ab7280, Abcam). Sections were mounted with medium containing DAPI (4′,6-diamidino-2-phenylindole; H-1200, Vector Laboratories). Sections were examined and imaged using a Nikon

A1 confocal imaging system. Analysis was carried out with the Nikon NIS-Elements software.

Ex vivo angiogenesis assay using mouse aortic rings

The mouse aortic ring assay was performed as described previously (*21*). Briefly, fresh isolated mouse aortas from WT and *Epac1*$^{-/-}$ mice were cleaned of periadventitial fat and connective tissues in minimum essential medium (MEM) and then cut into rings with a thickness of ~0.5 mm under a dissecting microscope using a surgical scalpel. The aortic rings were fast in MEM overnight and randomly placed into individual wells of a 96-well plate with 50 μl of collagen matrix (C3860, Sigma-Aldrich) on ice. Each 96-well plate was placed at room temperature for 15 min and then incubated for 1 hour at 37°C in a 5% CO_2 humidified incubator. Culture medium (150 μl) supplemented with VEGF (30 ng/ml) was added into each well and changed every other day. To test the effect of Epac inhibition, aortic rings isolated from WT mice were randomly divided into four groups and treated with vehicle control, 2.5, 5, or 10 μM Epac-specific inhibitor ESI-09 (*22*, *23*). To test the rescue effect of DAPT (S2215, Selleck Chemical, Houston, TX), aortic rings isolated from *Epac1* KO mice were randomly divided into two groups and treated with vehicle control or 10 μM DAPT, respectively. Both ESI-09 and DAPT were refreshed every other day along with medium change. After 6 to 7 days, microvessel sprouting was observed and imaged using an inverted phase-contrast microscope. For quantification of microvessel sprouts, images were sharpened and contrast-enhanced using ImageJ to improve visibility. Images were subsequently imported in GIMP (GNU Image Manipulation Program) to generate a binary image by setting the intensity threshold at 180 across all photos. Microvessel sprouts were then traced and validated by comparing with the original image. The number of the main outgrowths from each aortic ring was used for data analysis.

Cell culture and treatment

HUVECs (CC-3124) were from Lonza (Allendale, NJ) and cultured in Endothelial Cell Growth Medium (EGM; Lonza). Human dermal neonatal fibroblasts (HDFNs) were purchased from Cascade Biologics (Portland, OR) and cultured in Dulbecco's modified Eagle's medium (DMEM; D5030, Sigma-Aldrich) supplemented with 5% fetal bovine serum (FBS; Hyclone, Logan, UT), 2 mM glutamine, 1 mM sodium pyruvate, and penicillin-streptomycin (100 U/ml; P4333, Sigma-Aldrich). Human primary retinal microvascular ECs (HRMECs) were purchased from Cell Biologics (Chicago, IL) and cultured in basal Human Endothelial Cell Medium (Cell Biologics) supplemented with Supplement Kit and 10% FBS (Cell Biologics). Cell cultures were maintained at 37°C in 5% CO_2 humidified incubators. Cells from passages between 3 and 8 were used for all experiments described in this study. For pharmacological manipulations, near-confluent HUVECs were washed once with Hanks' Balanced Salt solution (HBSS) and starved in serum-free endothelial basal medium (EBM) for 2 hours followed by the treatment of control vehicle (5 μM 007-AM; C051, BioLog Life Science Institute, Bremen, Germany), recombinant VEGF (rVEGF, 10 ng/ml), or 007-AM and rVEGF for various time intervals. For experiments involving RNA interference (RNAi), HUVECs at 70% confluence were transfected with Epac1-specific (1299001) or nontargeting control (12935-300; Thermo Fisher Scientific) Stealth RNAi siRNA oligonucleotides at a final concentration of 50 nM using Lipofectamine 2000 (Thermo Fisher Scientific) according to the manufacturer's instructions. Forty-eight hours after transfection, cells were starved in serum-free EBM for 2 hours followed by treatment of control vehicle, rVEGF (10 ng/ml), or 10 μM DAPT for various time intervals. Ectopic expression of Rap1GAP in HUVECs was achieved by transfection of the pFLAG-CMV2-Rap1GAP vector (*58*) using Lipofectamine 2000.

MTS cell proliferation assay

After HRMECs were cultured and plated in a 96-well plate in basal Human Endothelial Cell Medium supplemented with Supplement Kit and 10% FBS for 24 hours, culture medium was changed to basal medium supplemented with VEGF (30 ng/ml), or 2.5 μM 007-AM or 2.5 μM ESI-09 or combination for 16 hours. Next, culture medium was changed to basal medium, and 20 μl of CellTiter 96 AQ_{ueous} One Solution Reagent from CellTiter 96 AQ_{ueous} One Solution Cell Proliferation Assay (MTS) kit (Promega, Madison, WI) was added into each well and incubated for 1.5 hours at 37°C, followed by measurement of absorbance at 490 nm.

Scratch wound healing assay

HRMECs were seeded in collagen-coated 24-well plates at a density of 8×10^4 cells per well. The next day, HRMECs were serum-starved for 6 hours. Confluent cell monolayer were then scraped with a 200-μl pipette tip to generate scratch wounds and washed with PBS to remove cell debris. Cells were incubated at 37°C for 16 hours in serum-free medium supplemented with VEGF (30 ng/ml) or 5 μM 007-AM or 2.5 μM ESI-09 or combination. Images of cells were taken with a Leica microscope immediately and 16 hours after scratching.

Cell invasion assay

Cell invasion was analyzed by using the BioCoat Matrigel Invasion Chamber (Corning, Steuben County, NY) according to the manufacturer's instructions. Briefly, HRMECs were serum-starved for 24 hours, cells were resuspended in serum-free media supplemented with vehicle [dimethyl sulfoxide (DMSO)] or ESI-09 or 007-AM, and 4×10^4 cells per well for ESI-09 or 2×10^4 cells per well for 007-AM were plated in the upper insert. Medium with 2% FBS was supplemented with vehicle (DMSO) or 5 μM 007-AM or 2.5 μM ESI-09 and added to the lower wells. After cells were incubated for 20 hours, noninvading cells were gently scrubbed off the upper surface. Migrated cells adhering to the lower membrane were fixed in 4% PFA and stained with 0.1% crystal violet solution. The average number of migrated cells was quantified by counting cells in six randomly selected fields.

EC tube formation assay

Growth factor–reduced basement membrane matrix (Corning) was diluted with basal medium (1:1) on ice, and diluted matrix (100 μl per well) was added to a 48-well plate on ice and allowed to polymerize at 37°C for 45 min. Subsequently, 5×10^4 HRMECs were prepared in 400 μl of basal medium supplemented with VEGF (30 ng/ml) or 2.5 μM 007-AM or 2.5 μM ESI-09 or combination and plated onto the surface of the Matrigel. After the cells were incubated for 5 hours at 37°C, images of the tubular structures were taken by a Leica microscope.

In vitro 3D angiogenesis assay

Angiogenesis assay was performed as previously described (*59*). Briefly, collagen/media solution was prepared on ice and mixed with HUVECs (1×10^6/ml) and/or HDFNs (5×10^5/ml). Subsequently, 30 μl of collagen/cell mixture was spotted onto a 5-mm woven nylon

mesh ring (Tetko Inc., Elmford, NY). After the collagen/cell mixture was polymerized at 37°C, samples were transferred to a 96-well flat-bottom culture plate with media. The culture media consisted of EBM-2 supplemented with all "bullet kit" components except FBS, VEGF, and basic FGF. This basic media was supplemented with 1% FBS and VEGF (30 ng/ml). For Epac inhibition, 2.5 μM ESI-09 was added to the culture media, which was refreshed every day. For coculture assay, HUVECs were transiently transfected using HiPerFect (QIAGEN, Valencia, CA) with Epac1 siRNA (M007676-01-0005, Dharmacon, Lafayette, CO). On day 5, collagen-embedded cells were fixed in 4% PFA and stained with tetramethyl rhodamine isothiocyanate–labeled lectin (10 μg/ml; *Ulex europaeus*, UEA-I, Sigma-Aldrich) overnight. Images were taken by a Zeiss LSM confocal microscope.

Western blot analysis

Cells were lysed in 1× Cell Lysis Buffer (Cell Signaling Technology, Beverly, MA) supplemented with phenylmethylsulfonyl fluoride (PMSF) and cOmplete, Mini, EDTA-free Protease Inhibitor Cocktail Tablet (Roche, Indianapolis, IN). Cell lysates with 5 to 10 μg of total proteins were resolved on stain-free SDS–polyacrylamide gels containing 0.05% 2, 2, 2-trichloroethanol. After electrophoresis, images were taken by ChemiDoc Touch Imaging System (Bio-Rad, Hercules, CA) for total protein loading quantification before proteins were transferred to a polyvinylidene difluoride membrane (Millipore). After blocking with 5% nonfat milk, the blots were first incubated with primary antibodies against Akt (no. 9272), Epac1 (no. 4155), DLL4 (no. 2589), Notch1 (no. 3608), NICD (no. 4147), phospho-Akt (S473) (no. 4060), phospho-eNOS (no. 9571), PS1 (no. 5643), GAPDH (glyceraldehyde-3-phosphate dehydrogenase; no. 2118) (Cell Signaling Technology), eNOS (no. 610297, BD Biosciences), or α-tubulin (T6074, Sigma-Aldrich) at 4°C for overnight and then followed by incubation with horseradish peroxidase–conjugated secondary antibodies (Cell Signaling Technology) and detection using Amersham ECL Prime Western Blotting Detection Reagent (GE Healthcare Life Sciences, Pittsburgh, PA). The intensity of the signals was assessed with ChemiDoc Touch Imaging System and quantitated with Image Lab Software (Bio-Rad) or ImageJ software. Protein levels were normalized against total protein loading or an internal control such as GAPDH or α-tubulin. The sample readout was determined as a ratio by dividing the normalized protein level in the treatment cells with that in the control cells, which was set to be 1. Statistical analysis was performed using data from at least three independent experiments.

Real-time polymerase chain reaction

Total RNA from HUVECs was extracted with RNeasy Mini Kit (QIAGEN) according to the manufacturer's instruction. Complementary DNA (cDNA) was prepared using The High Capacity cDNA Reverse Transcription kit (Applied Biosystems, Waltham, MA) or Moloney murine leukemia virus reverse transcriptase (Invitrogen, Carlsbad, CA). Real-time polymerase chain reaction (PCR) analysis was performed using iQ SYBR Green Supermix (Bio-Rad) or a StepOne PCR system (Applied Biosystems) with Power SYBR Green according to the manufacturers' recommendations. The sequence (5′-3′) of forward and reverse primers used for real-time PCR are the following: human transcripts: Epac1, CCTCTCCAACTCGGTGAAGC (forward) and CTGGCTGAACAACACGGTC (reverse); Hes1, AGCACACTTGGGTCTGTGC (forward) and TGAAGAAAGATAGCTCGCGG (reverse); Hey1, ATCTGCTAAGCTAGAAAAAGCCG (forward) and GTGCGCGTCAAAGTAACCT (reverse); DLL4, CTGGAGCTCAGCGAGTGTGAC (forward) and CCTGGTCCTTACAGCTGCCTC (reverse); and GAPDH, CTGACTTCAACAGCGACACC (forward) and GTGGTCCAGGGGGTCTTACTC (reverse). Mouse transcripts: Epac1, AATGGCTGTGGGAACGTATCTC (forward) and CCTGGTTAGGGAGCCAAACA (reverse); Epac2, TGCAAACACTGCCAGAACAGT (forward) and GAGCGGCATCCGGATTG (reverse); PKA, AGTACTTGGCCCCCGAGATT (forward) and ACCAGTCCACAG CCTTGTTGT (reverse); PDE1a, AGGTCGGACGTTGCTATTCTGT (forward) and CGCTGACGTGGTGATTCTCA (reverse); PDE1b, GTTCCGAAGCATCGTGCAT (forward) and GAACATCCGCTCCACGAAGA (reverse); PDE3a, CCTGGCCGACCCTTCTCT (forward) and AGTTGCTTACGGCCCTCAAG (reverse); PDE3b, GAATTCTGGAGGTGGAAATGGA (forward) and TCTGACACCATATTGCGAGCTT (reverse); DLL4, GACCTGCGGCCAGAGACTT (forward) and GAGCCTTGGATGATGATTTGG (reverse); Hes1, CCCCAGCCAGTGTCAACAC (forward) and TGTGCTCAGAGGCCGTCTT (reverse); Hey1, TCACCTGAAAATGCTGCACACT (forward) and GGCGTGCGCGTCAAA (reverse); and Hprt, GAAAGACTTGCTCGAGATGTCATG (forward) and CACACAGAGGGCCACAATGT (reverse). The fold difference was calculated by the ΔΔCT method using GAPDH or Hprt as the internal control.

Epac1 affinity pull-down

HeLa S3 cells stably expressing Epac1 fused with a C-terminal FLAG/hemagglutinin tandem epitope tag were generated and maintained in DMEM supplemented with 10% FBS as previously described (*60*). Cells from 10-cm plates with 90% confluency were lysed in lysis buffer containing 25 mM tris (pH 7.6), 150 mM NaCl, 5 mM $MgCl_2$, 1% Triton X-100, and PMSF and protease inhibitors. Cell lysate was incubated with Anti-FLAG M2 affinity gel (A2220, Sigma-Aldrich) overnight at 4°C with constant gentle mixing and then washed five times with lysis buffer and 10% glycerol. Cellular Epac1-FLAG complexes were eluted with a purified FLAG peptide in lysis buffer. Control pulldown was performed using cell lysate with equal total cellular proteins from cells stably transfected with the empty vector. Interaction between Epac1 and γ-secretase was further confirmed by affinity pulldown using recombinant GST-Epac1 that was purified as described previously (*61*). Briefly, HUVEC or HeLa total cell lysates were mixed with GST-Epac1 or GST control and incubated at 4°C with constant gentle mixing for 2 hours. GST-Epac1 or GST was recovered using glutathione–agarose beads. Cellular binding partners were eluted by glutathione solution after extensive washing of the beads.

γ-Secretase activity assay

The exo-cell assay was performed as described previously (*28*). Briefly, cells were seeded in 12-well culture plates for 24 hours, and media were removed and washed twice with HBSS and once with serum-free media. Then cells were incubated in serum-free media before 007-AM (5 μM) activation at each indicated time point. Next, recombinant Notch substrate (0.4 μM) was added in Pipes buffer [50 mM Pipes (pH 7.0), 150 mM KCl, 5 mM $CaCl_2$, and 5 mM $MgCl_2$] and 0.25% CHAPSO [3-([3-Cholamidopropyl]dimethylammonio)-2-hydroxy-1-propanesulfonate] detergent and incubated at 37°C for 3 hours. γ-Secretase products were detected by AlphaLISA methods using SM320 antibody for NICD (*62*). Activity readout is presented as arbitrary AlphaLISA units. The assay background was defined in the presence of a γ-secretase inhibitor and subtracted from activity assays. Specific activity was normalized to protein concentration.

γ-Secretase internalization assay

To monitor the effect of Epac1 activation on γ-secretase internalization, we first biotinylated the cell surface proteins using a Pierce Cell Surface Isolation Kit (89881, Thermo Fisher Scientific) and then followed the γ-secretase internalization by NeutrAvidin pulldown and immunoblotting. Briefly, HUVECs were grown in EGM in 10-cm dishes to 90 to 100% confluence and starved in serum-free EBM for 1.5 hours. The cells were quickly washed twice with 5 ml of ice-cold PBS supplemented with 0.1 mM $CaCl_2$ and 1 mM $MgCl_2$ and then incubated with 7.5 ml of EZ-Link Sulfo-NHS-SS-Biotin (0.25 mg/ml) in ice-cold PBS for 30 min at 4°C in the dark on a shaker. Quench solution (450 μl) was added to the cells to stop the biotinylation reaction. The cells were washed with 5 ml of PBS twice to remove residual unreacted biotin and then brought to 37°C in 5 ml of EBM for 10 min followed by treating with 5 μM 007-AM or DMSO vehicle for 12 min at 37°C. After incubation, cells were placed back on ice to halt endocytosis. After washing with cold PBS twice, residual surface biotinylation was removed by incubating with 7.5 ml of glutathione-stripping buffer [75 mM NaCl, 1 mM $MgCl_2$, 0.1 mM $CaCl_2$, 50 mM glutathione, 80 mM NaOH, and 10% FBS (pH 8.6)] at 4°C for 30 min. The cells were lysed with 300 μl of radioimmunoprecipitation assay buffer with protease inhibitor cocktail and 1 mM PMSF after washing with 5 ml of ice-cold PBS three times. The internalized surface proteins were captured by NeutrAvidin Agarose beads following the manufacturer's instruction. The levels of internalized γ-secretase were probed by immunoblotting using PS1 antibody.

Statistics

All data were expressed as means ± SEM, unless stated otherwise, and analyzed using unpaired Student's *t* test with Welch's correction for comparison between two groups or ordinary one-way analysis of variance (ANOVA) with Dunnett's multiple comparisons test with the Geisser-Greenhouse correction for more than two groups. Differences were considered significant if $P < 0.05$. Cell culture experiments were repeated at least three times.

SUPPLEMENTARY MATERIALS

Supplementary material for this article is available at http://advances.sciencemag.org/cgi/content/full/6/1/eaay3566/DC1

Fig. S1. Epac1 deletion does not compromise physiological angiogenesis in vivo.
Fig. S2. Gene expression of signaling molecules related to cAMP pathway in mouse retinal vasculature in OIR model.
Fig. S3. Epac2 deletion has no effect on OIR-induced neovascularization.
Fig. S4. Epac1 deletion decreases the proliferation in retinal vasculature of OIR.
Fig. S5. Epac1 inhibition suppresses microvessel sprouting from aortic rings.
Fig. S6. Epac1 cross-talks with VEGF signaling and regulates EC functions.
Fig. S7. Increased Notch target gene expression in Epac1-deficient vessels.
Fig. S8. Cellular γ-secretase activity in response to Epac activation and inhibition in parental HeLa cells.
Fig. S9. Inhibition of γ-secretase by DAPT neutralizes Epac1 siRNA-mediated Notch activation.
Fig. S10. Inhibition of γ-secretase by DAPT rescues defective microvessel sprouting in Epac1 KO aortic rings.

REFERENCES AND NOTES

1. P. Carmeliet, Angiogenesis in life, disease and medicine. *Nature* **438**, 932–936 (2005).
2. X. Cheng, Z. Ji, T. Tsalkova, F. Mei, Epac and PKA: A tale of two intracellular cAMP receptors. *Acta Biochim. Biophys. Sin.* **40**, 651–662 (2008).
3. J. de Rooij, F. J. T. Zwartkruis, M. H. G. Verheijen, R. H. Cool, S. M. B. Nijman, A. Wittinghofer, J. L. Bos, Epac is a Rap1 guanine-nucleotide-exchange factor directly activated by cyclic AMP. *Nature* **396**, 474–477 (1998).
4. H. Kawasaki, G. M. Springett, N. Mochizuki, S. Toki, M. Nakaya, M. Matsuda, D. E. Housman, A. M. Graybiel, A family of cAMP-binding proteins that directly activate Rap1. *Science* **282**, 2275–2279 (1998).
5. W. G. Robichaux III, X. Cheng, Intracellular cAMP Sensor EPAC: Physiology, pathophysiology, and therapeutics development. *Physiol. Rev.* **98**, 919–1053 (2018).
6. O. L. Roberts, C. Dart, cAMP signalling in the vasculature: The role of Epac (exchange protein directly activated by cAMP). *Biochem. Soc. Trans.* **42**, 89–97 (2014).
7. S. J. Netherton, J. A. Sutton, L. S. Wilson, R. L. Carter, D. H. Maurice, Both protein kinase A and exchange protein activated by cAMP coordinate adhesion of human vascular endothelial cells. *Circ. Res.* **101**, 768–776 (2007).
8. M. R. Kooistra, M. Corada, E. Dejana, J. L. Bos, Epac1 regulates integrity of endothelial cell junctions through VE-cadherin. *FEBS Lett.* **579**, 4966–4972 (2005).
9. X. Cullere, S. K. Shaw, L. Andersson, J. Hirahashi, F. W. Luscinskas, T. N. Mayadas, Regulation of vascular endothelial barrier function by Epac, a cAMP-activated exchange factor for Rap GTPase. *Blood* **105**, 1950–1955 (2005).
10. S. Fukuhara, A. Sakurai, H. Sano, A. Yamagishi, S. Somekawa, N. Takakura, Y. Saito, K. Kangawa, N. Mochizuki, Cyclic AMP potentiates vascular endothelial cadherin-mediated cell-cell contact to enhance endothelial barrier function through an Epac-Rap1 signaling pathway. *Mol. Cell. Biol.* **25**, 136–146 (2005).
11. K. W. van Hooren, E. L. van Agtmaal, M. Fernandez-Borja, J. A. van Mourik, J. Voorberg, R. Bierings, The Epac-Rap1 signaling pathway controls cAMP-mediated exocytosis of Weibel-Palade bodies in endothelial cells. *J. Biol. Chem.* **287**, 24713–24720 (2012).
12. W. Yang, F. C. Mei, X. Cheng, EPAC1 regulates endothelial annexin A2 cell surface translocation and plasminogen activation. *FASEB J.* **32**, 2212–2222 (2018).
13. R. K. Kopperud, C. B. Rygh, T. V. Karlsen, C. Krakstad, R. Kleppe, E. A. Hoivik, M. Bakke, O. Tenstad, F. Selheim, Å. Lidén, L. Madsen, T. Pavlin, T. Taxt, K. Kristiansen, F. E. Curry, R. K. Reed, S. O. Døskeland, Increased microvascular permeability in mice lacking Epac1 (Rapgef3). *Acta physiologica* **219**, 441–452 (2017).
14. B. Gong, T. Shelite, F. C. Mei, T. Ha, Y. Hu, G. Xu, Q. Chang, M. Wakamiya, T. G. Ksiazek, P. J. Boor, D. H. Bouyer, V. L. Popov, J. Chen, D. H. Walker, X. Cheng, Exchange protein directly activated by cAMP plays a critical role in bacterial invasion during fatal rickettsioses. *Proc. Natl. Acad. Sci. U.S.A.* **110**, 19615–19620 (2013).
15. J. Garg, Y. X. Feng, S. R. Jansen, J. Friedrich, F. Lezoualc'h, M. Schmidt, T. Wieland, Catecholamines facilitate VEGF-dependent angiogenesis via β2-adrenoceptor-induced Epac1 and PKA activation. *Oncotarget* **8**, 44732–44748 (2017).
16. L. Liu, Y. Jiang, J. J. Steinle, Epac1 protects the retina against ischemia/reperfusion-induced neuronal and vascular damage. *PLOS ONE* **13**, e0204346 (2018).
17. L. E. Smith, E. Wesolowski, A. McLellan, S. K. Kostyk, R. D'Amato, R. Sullivan, P. A. D'Amore, Oxygen-induced retinopathy in the mouse. *Invest. Ophthalmol. Vis. Sci.* **35**, 101–111 (1994).
18. H. Ameri, H. Liu, R. Liu, Y. Ha, A. A. Paulucci-Holthauzen, S. Hu, M. Motamedi, B. F. Godley, R. G. Tilton, W. Zhang, TWEAK/Fn14 pathway is a novel mediator of retinal neovascularization. *Invest. Ophthalmol. Vis. Sci.* **55**, 801–813 (2014).
19. L. E. H. Smith, W. Shen, C. Perruzzi, S. Soker, F. Kinose, X. Xu, G. Robinson, S. Driver, J. Bischoff, B. Zhang, J. M. Schaeffer, D. R. Senger, Regulation of vascular endothelial growth factor-dependent retinal neovascularization by insulin-like growth factor-1 receptor. *Nat. Med.* **5**, 1390–1395 (1999).
20. H. Wang, W. G. Robichaux, Z. Wang, F. C. Mei, M. Cai, G. du, J. Chen, X. Cheng, Inhibition of Epac1 suppresses mitochondrial fission and reduces neointima formation induced by vascular injury. *Sci. Rep.* **6**, 36552 (2016).
21. M. Baker, S. D. Robinson, T. Lechertier, P. R. Barber, B. Tavora, G. D'Amico, D. T. Jones, B. Vojnovic, K. Hodivala-Dilke, Use of the mouse aortic ring assay to study angiogenesis. *Nat. Protoc.* **7**, 89–104 (2011).
22. M. Almahariq, T. Tsalkova, F. C. Mei, H. Chen, J. Zhou, S. K. Sastry, F. Schwede, X. Cheng, A novel EPAC-specific inhibitor suppresses pancreatic cancer cell migration and invasion. *Mol. Pharmacol.* **83**, 122–128 (2013).
23. Y. Zhu, H. Chen, S. Boulton, F. Mei, N. Ye, G. Melacini, J. Zhou, X. Cheng, Biochemical and pharmacological characterizations of ESI-09 based EPAC inhibitors: Defining the ESI-09 "therapeutic window". *Sci. Rep.* **5**, 9344 (2015).
24. Y. Hu, W. G. Robichaux III, F. C. Mei, E. R. Kim, H. Wang, Q. Tong, J. Jin, M. Xu, J. Chen, X. Cheng, Role of exchange protein directly activated by Cyclic AMP isoform 1 in energy homeostasis: Regulation of leptin expression and secretion in white adipose tissue. *Mol. Cell. Biol.* **36**, 2440–2450 (2016).
25. R. Benedito, C. Roca, I. Sörensen, S. Adams, A. Gossler, M. Fruttiger, R. H. Adams, The notch ligands Dll4 and Jagged1 have opposing effects on angiogenesis. *Cell* **137**, 1124–1135 (2009).
26. J. Ridgway, G. Zhang, Y. Wu, S. Stawicki, W. C. Liang, Y. Chanthery, J. Kowalski, R. J. Watts, C. Callahan, I. Kasman, M. Singh, M. Chien, C. Tan, J. A. S. Hongo, F. de Sauvage, G. Plowman, M. Yan, Inhibition of Dll4 signalling inhibits tumour growth by deregulating angiogenesis. *Nature* **444**, 1083–1087 (2006).
27. B. De Strooper, W. Annaert, P. Cupers, P. Saftig, K. Craessaerts, J. S. Mumm, E. H. Schroeter, V. Schrijvers, M. S. Wolfe, W. J. Ray, A. Goate, R. Kopan, A presenilin-1-dependent

gamma-secretase-like protease mediates release of Notch intracellular domain. *Nature* **398**, 518–522 (1999).
28. C. C. Shelton, Y. Tian, M. G. Frattini, Y. M. Li, An exo-cell assay for examining real-time γ-secretase activity and inhibition. *Mol. Neurodegener.* **4**, 22 (2009).
29. N. Gupta-Rossi, E. Six, O. LeBail, F. Logeat, P. Chastagner, A. Olry, A. Israël, C. Brou, Monoubiquitination and endocytosis direct γ-secretase cleavage of activated Notch receptor. *J. Cell Biol.* **166**, 73–83 (2004).
30. S. Urra, C. A. Escudero, P. Ramos, F. Lisbona, E. Allende, P. Covarrubias, J. I. Parraguez, N. Zampieri, M. V. Chao, W. Annaert, F. C. Bronfman, TrkA receptor activation by nerve growth factor induces shedding of the p75 neurotrophin receptor followed by endosomal gamma-secretase-mediated release of the p75 intracellular domain. *J. Biol. Chem.* **282**, 7606–7615 (2007).
31. T. Vaccari, H. Lu, R. Kanwar, M. E. Fortini, D. Bilder, Endosomal entry regulates Notch receptor activation in Drosophila melanogaster. *J. Cell Biol.* **180**, 755–762 (2008).
32. M. T. Lai, E. Chen, M. C. Crouthamel, J. DiMuzio-Mower, M. Xu, Q. Huang, E. Price, R. B. Register, X. P. Shi, D. B. Donoviel, A. Bernstein, D. Hazuda, S. J. Gardell, Y. M. Li, Presenilin-1 and presenilin-2 exhibit distinct yet overlapping γ-secretase activities. *J. Biol. Chem.* **278**, 22475–22481 (2003).
33. Y. Liu, Y. W. Zhang, X. Wang, H. Zhang, X. You, F. F. Liao, H. Xu, Intracellular trafficking of presenilin 1 is regulated by beta-amyloid precursor protein and phospholipase D1. *J. Biol. Chem.* **284**, 12145–12152 (2009).
34. H. F. Dovey, V. John, J. P. Anderson, L. Z. Chen, P. de Saint Andrieu, L. Y. Fang, S. B. Freedman, B. Folmer, E. Goldbach, E. J. Holsztynska, K. L. Hu, K. L. Johnson-Wood, S. L. Kennedy, D. Kholodenko, J. E. Knops, L. H. Latimer, M. Lee, Z. Liao, I. M. Lieberburg, R. N. Motter, L. C. Mutter, J. Nietz, K. P. Quinn, K. L. Sacchi, P. A. Seubert, G. M. Shopp, E. D. Thorsett, J. S. Tung, J. Wu, S. Yang, C. T. Yin, D. B. Schenk, P. C. May, L. D. Altstiel, M. H. Bender, L. N. Boggs, T. C. Britton, J. C. Clemens, D. L. Czilli, D. Dieckman-McGinty, J. J. Droste, K. S. Fuson, B. D. Gitter, P. A. Hyslop, E. M. Johnstone, W. Y. Li, S. P. Little, T. E. Mabry, F. D. Miller, J. E. Audia, Functional γ-secretase inhibitors reduce β-amyloid peptide levels in brain. *J. Neurochem.* **76**, 173–181 (2001).
35. J. Yan, F. C. Mei, H. Cheng, D. H. Lao, Y. Hu, J. Wei, I. Patrikeev, D. Hao, S. J. Stutz, K. T. Dineley, M. Motamedi, J. D. Hommel, K. A. Cunningham, J. Chen, X. Cheng, Enhanced leptin sensitivity, reduced adiposity, and improved glucose homeostasis in mice lacking exchange protein directly activated by cyclic AMP isoform 1. *Mol. Cell. Biol.* **33**, 918–926 (2013).
36. A. B. Fulton, R. M. Hansen, A. Moskowitz, J. D. Akula, The neurovascular retina in retinopathy of prematurity. *Prog. Retin. Eye Res.* **28**, 452–482 (2009).
37. Z. Liu, S. Yan, J. Wang, Y. Xu, Y. Wang, S. Zhang, X. Xu, Q. Yang, X. Zeng, Y. Zhou, X. Gu, S. Lu, Z. Fu, D. J. Fulton, N. L. Weintraub, R. B. Caldwell, W. Zhang, C. Wu, X. L. Liu, J. F. Chen, A. Ahmad, I. Kaddour-Djebbar, M. Al-Shabrawey, Q. Li, X. Jiang, Y. Sun, A. Sodhi, L. Smith, M. Hong, Y. Huo, Endothelial adenosine A2a receptor-mediated glycolysis is essential for pathological retinal angiogenesis. *Nat. Commun.* **8**, 584 (2017).
38. X. L. Liu, R. Zhou, Q. Q. Pan, X. L. Jia, W. N. Gao, J. Wu, J. Lin, J. F. Chen, Genetic inactivation of the adenosine A2A receptor attenuates pathologic but not developmental angiogenesis in the mouse retina. *Invest. Ophthalmol. Vis. Sci.* **51**, 6625–6632 (2010).
39. D. Martini, M. D. Monte, C. Ristori, E. Cupisti, S. Mei, P. Fiorini, L. Filippi, P. Bagnoli, Antiangiogenic effects of β2-adrenergic receptor blockade in a mouse model of oxygen-induced retinopathy. *J. Neurochem.* **119**, 1317–1329 (2011).
40. M. Dal Monte, C. Ristori, M. Cammalleri, P. Bagnoli, Effects of somatostatin analogues on retinal angiogenesis in a mouse model of oxygen-induced retinopathy: Involvement of the somatostatin receptor subtype 2. *Invest. Ophthalmol. Vis. Sci.* **50**, 3596–3606 (2009).
41. D. Wang, R. N. DuBois, Cyclooxygenase 2-derived prostaglandin E2 regulates the angiogenic switch. *Proc. Natl. Acad. Sci. U.S.A.* **101**, 415–416 (2004).
42. R. Rao, R. Redha, I. Macias-Perez, Y. Su, C. Hao, R. Zent, M. D. Breyer, A. Pozzi, Prostaglandin E2-EP4 receptor promotes endothelial cell migration via ERK activation and angiogenesis in vivo. *J. Biol. Chem.* **282**, 16959–16968 (2007).
43. P. Carmeliet, Mechanisms of angiogenesis and arteriogenesis. *Nat. Med.* **6**, 389–395 (2000).
44. M. Lohela, M. Bry, T. Tammela, K. Alitalo, VEGFs and receptors involved in angiogenesis versus lymphangiogenesis. *Curr. Opin. Cell Biol.* **21**, 154–165 (2009).
45. N. Ferrara, H. P. Gerber, J. LeCouter, The biology of VEGF and its receptors. *Nat. Med.* **9**, 669–676 (2003).
46. A. F. Siekmann, N. D. Lawson, Notch signalling limits angiogenic cell behaviour in developing zebrafish arteries. *Nature* **445**, 781–784 (2007).
47. H. Gerhardt, M. Golding, M. Fruttiger, C. Ruhrberg, A. Lundkvist, A. Abramsson, M. Jeltsch, C. Mitchell, K. Alitalo, D. Shima, C. Betsholtz, VEGF guides angiogenic sprouting utilizing endothelial tip cell filopodia. *J. Cell Biol.* **161**, 1163–1177 (2003).
48. L. Jakobsson, C. A. Franco, K. Bentley, R. T. Collins, B. Ponsioen, I. M. Aspalter, I. Rosewell, M. Busse, G. Thurston, A. Medvinsky, S. Schulte-Merker, H. Gerhardt, Endothelial cells dynamically compete for the tip cell position during angiogenic sprouting. *Nat. Cell Biol.* **12**, 943–953 (2010).
49. F. C. Mei, J. Qiao, O. M. Tsygankova, J. L. Meinkoth, L. A. Quilliam, X. Cheng, Differential signaling of cyclic AMP: Opposing effects of exchange protein directly activated by cyclic AMP and cAMP-dependent protein kinase on protein kinase B activation. *J. Biol. Chem.* **277**, 11497–11504 (2002).
50. S. Namkoong, C. K. Kim, Y. L. Cho, J. H. Kim, H. Lee, K. S. Ha, J. Choe, P. H. Kim, M. H. Won, Y. G. Kwon, E. B. Shim, Y. M. Kim, Forskolin increases angiogenesis through the coordinated cross-talk of PKA-dependent VEGF expression and Epac-mediated PI3K/Akt/eNOS signaling. *Cell. Signal.* **21**, 906–915 (2009).
51. F. Chen, H. Hasegawa, G. Schmitt-Ulms, T. Kawarai, C. Bohm, T. Katayama, Y. Gu, N. Sanjo, M. Glista, E. Rogaeva, Y. Wakutani, R. Pardossi-Piquard, X. Ruan, A. Tandon, F. Checler, P. Marambaud, K. Hansen, D. Westaway, P. St George-Hyslop, P. Fraser, TMP21 is a presenilin complex component that modulates γ-secretase but not epsilon-secretase activity. *Nature* **440**, 1208–1212 (2006).
52. S. Zhou, H. Zhou, P. J. Walian, B. K. Jap, CD147 is a regulatory subunit of the gamma-secretase complex in Alzheimer's disease amyloid β-peptide production. *Proc. Natl. Acad. Sci. U.S.A.* **102**, 7499–7504 (2005).
53. J. C. Villa, D. Chiu, A. H. Brandes, F. E. Escorcia, C. H. Villa, W. F. Maguire, C. J. Hu, E. de Stanchina, M. C. Simon, S. S. Sisodia, D. A. Scheinberg, Y. M. Li, Nontranscriptional role of Hif-1α in activation of γ-secretase and notch signaling in breast cancer. *Cell Rep.* **8**, 1077–1092 (2014).
54. C. J. Ramos, C. Lin, X. Liu, D. A. Antonetti, The EPAC-Rap1 pathway prevents and reverses cytokine-induced retinal vascular permeability. *J. Biol. Chem.* **293**, 717–730 (2018).
55. J. Li, R. Zhang, C. Wang, X. Wang, M. Xu, J. Ma, Q. Shang, Activation of the small GTPase Rap1 inhibits choroidal neovascularization by regulating cell junctions and ROS generation in rats. *Curr. Eye Res.* **43**, 934–940 (2018).
56. L. Pereira, H. Cheng, D. H. Lao, L. Na, R. J. van Oort, J. H. Brown, X. H. T. Wehrens, J. Chen, D. M. Bers, Epac2 mediates cardiac β1-adrenergic-dependent sarcoplasmic reticulum Ca2+ leak and arrhythmia. *Circulation* **127**, 913–922 (2013).
57. H. Liu, W. Zhang, Z. Xu, R. W. Caldwell, R. B. Caldwell, S. E. Brooks, Hyperoxia causes regression of vitreous neovascularization by downregulating VEGF/VEGFR2 pathway. *Invest. Ophthalmol. Vis. Sci.* **54**, 918–931 (2013).
58. A. F. Castro, J. F. Rebhun, G. J. Clark, L. A. Quilliam, Rheb binds tuberous sclerosis complex 2 (TSC2) and promotes S6 kinase activation in a rapamycin- and farnesylation-dependent manner. *J. Biol. Chem.* **278**, 32493–32496 (2003).
59. H. Liu, S. Kennard, B. Lilly, NOTCH3 expression is induced in mural cells through an autoregulatory loop that requires endothelial-expressed JAGGED1. *Circ. Res.* **104**, 466–475 (2009).
60. F. C. Mei, X. Cheng, Interplay between exchange protein directly activated by cAMP (Epac) and microtubule cytoskeleton. *Mol. Biosyst.* **1**, 325–331 (2005).
61. T. Tsalkova, F. C. Mei, S. Li, O. G. Chepurny, C. A. Leech, T. Liu, G. G. Holz, V. L. Woods, X. Cheng, Isoform-specific antagonists of exchange proteins directly activated by cAMP. *Proc. Natl. Acad. Sci. U.S.A.* **109**, 18613–18618 (2012).
62. D. M. Chau, C. J. Crump, J. C. Villa, D. A. Scheinberg, Y. M. Li, Familial Alzheimer disease presenilin-1 mutations alter the active site conformation of γ-secretase. *J. Biol. Chem.* **287**, 17288–17296 (2012).

Acknowledgments: We thank K. Levental and W. Robichaux for assistance in image analysis and W. Robichaux and W. Lin for helpful discussions. **Funding:** This work was supported by grants from the National Institutes of Health (R35GM122536 to X.C., R01EY026629 to W.Z., and R01NS096275 and RF1AG057593 to Y.-M.L.), the American Heart Association (15POST22450025 and 17SDG33630151 to H.L.), the Retina Research Foundation (to W.Z.) and the JPB Foundation (to Y.-M.L.). The authors also acknowledge the MSK Cancer Center Support Grant/Core Grant (grant P30 CA008748). The funders had no role in the study design, data collection and analysis, decision to publish, or preparation of the manuscript. **Author contributions:** H.L., F.C.M., W.Y., H.W., E.W., Y.-M.L., W.Z., and X.C. designed the experiments. H.L., F.C.M., W.Y., H.W., J.C., E.W., P.L., and X.C. performed the experiments. H.L., F.C.M., W.Y., H.W., J.C., E.W., E.T., Y.-M.L., W.Z., and X.C. analyzed the data. H.L., F.C.M., W.Y., E.W., Y.-M.L., W.Z., and X.C. wrote the manuscript. **Competing interests:** The authors declare that they have no competing interests. **Data and materials availability:** All data needed to evaluate the conclusions in the paper are present in the paper and/or the Supplementary Materials. Additional data related to this paper may be requested from the authors.

Submitted 11 June 2019
Accepted 29 October 2019
Published 1 January 2020
10.1126/sciadv.aay3566

Citation: H. Liu, F. C. Mei, W. Yang, H. Wang, E. Wong, J. Cai, E. Toth, P. Luo, Y.-M. Li, W. Zhang, X. Cheng, Epac1 inhibition ameliorates pathological angiogenesis through coordinated activation of Notch and suppression of VEGF signaling. *Sci. Adv.* **6**, eaay3566 (2020).